# Molecular dynamics simulations of lattice thermal conductivity of bismuth telluride using two-body interatomic potentials

Bo Qiu and Xiulin Ruan*

*School of Mechanical Engineering and the Birck Nanotechnology Center, Purdue University, West Lafayette, Indiana 47907-2088, USA*

Two-body interatomic potentials in the Morse potential form have been developed for bismuth telluride, and the potentials are used in molecular dynamics simulations to predict the thermal conductivity. The density-functional theory with local-density approximations is first used to calculate the total energies for many artificially distorted $Bi_2Te_3$ configurations to produce the energy surface. Then by fitting to this energy surface and other experimental data, the Morse potential form is parameterized. The fitted empirical interatomic potentials are shown to reproduce the elastic and phonon data well. Molecular dynamics simulations are then performed to predict the thermal conductivity of bulk $Bi_2Te_3$ at different temperatures, and the results agree with experimental data well.

## I. INTRODUCTION

There has been renewed interest on high-performance thermoelectric materials in the last decades. Thermoelectric energy conversion can convert waste heat to electricity without any moving parts, therefore it could play a significant role in addressing the energy challenge. The effectiveness of a thermoelectric material is characterized by its figure of merit $ZT$ given by $ZT=S^2\sigma T/\kappa$, where $S$, $\sigma$, and $T$ are the Seebeck coefficient, electrical conductivity, and absolute temperature, respectively. Here $\kappa$ is the thermal conductivity which contains both electronic and lattice contributions $\kappa_e$ and $\kappa_l$. High-performance thermoelectric materials with high $ZT$ require high $S$ and $\sigma/\kappa$ ratio.

$Bi_2Te_3$ as well as its alloys have long been the best thermoelectric materials at room temperature with a $ZT$ around 1. In the last decade significant enhancement of $ZT$ has been achieved using nanostructures. A $ZT$ value of 2.4 was reported in a $p$-type superlattice based on $Bi_2Te_3$ and $Sb_2Te_3$ when heat flows in the cross-plane direction.[1] Bismuth telluride nanowires have been characterized for their enhanced properties.[2] More recently, a peak $ZT$ value of 1.4 at $T$ =100 K was achieved in nanostructured bismuth antimony telluride bulk alloys, which are made using ball milling and hot pressing the nanoparticles into bulk ingots.[3] And $Bi_2Te_3/Sb_2Te_3$ bulk nanocomposites with laminated structure was prepared by adopting a route involving hydrothermal synthesis and hot pressing to achieve $ZT$ value of 1.47 around 450 K.[4] The high $ZT$ values in these nanostructures is mostly attributed to the reduction in the lattice thermal conductivity.

Despite the rapid progress in experiments, theoretical studies on the thermal transport in both bulk and nanostructures of $Bi_2Te_3$ are rare,[5,6] largely due to its heavy metal elements and complicated crystal structure. So far, common theoretical approaches for phonon thermal conductivity include Boltzmann transport equation (BTE), Monte Carlo simulations, and molecular dynamics (MD) simulations. BTE and Monte Carlo methods rely on relaxation-time models to describe phonon scattering and they generally require fitting of certain parameters to experimental data.[6–8] Molecu-

lar dynamics does not need any prior knowledge of phonon transport from experiment—only the interatomic potentials are the inputs. However, the proper interatomic potentials are often difficult to obtain, which is the case for $Bi_2Te_3$. Only recently the first set of interatomic potentials for $Bi_2Te_3$ bulk crystal were developed by Huang *et al.*[5] and then used in equilibrium molecular dynamics simulations to predict the phonon thermal conductivity. Their prediction results agree with experimental data quite well, although the three-body potential forms are quite complicated.

In this work, we develop simple two-body interatomic potentials for $Bi_2Te_3$ using density-functional theory (DFT) and then use these potentials in molecular dynamics to predict the phonon thermal conductivity. We first perform *ab initio* calculations to obtain the ground-state energies of a series of distinct configurations. The energy surface data are then used to parameterize the Morse potential form through the least-square fitting. The obtained potentials are validated in lattice-dynamics calculations via reproducing the material's lattice and elastic properties. Molecular dynamics simulations together with the Green-Kubo method are performed and the lattice thermal conductivities are predicted over the temperature range of 150–500 K.

## II. ELECTRONIC STRUCTURE AND PHONON DENSITY OF STATES

Bulk $Bi_2Te_3$ belongs to the space group $D_{3d}^5(R\bar{3}m)$ with a rhombohedral lattice structure, along the trigonal axis of which atoms are in the sequence of Te1-Bi-Te2-Bi-Te1 (Fig. 1). The hexagonal conventional cell parameters are $a$ =4.369 Å and $c$=30.42 Å and the corresponding rhombohedral unit-cell parameters[9] are $a_R$=10.45 Å, $\theta_R$=24.13° with Te1 and Bi atoms sitting at $(\pm u, \pm u, \pm u)$ and $(\pm v, \pm v, \pm v)$, where $u$=0.399, $v$=0.792, respectively. To compute the electronic structure, *ab initio* calculations were performed employing the full-potential linearized augmented plane wave method[10] based on DFT (Ref. 11) using the code WIEN2K.[12] Due to the large atomic mass of Bi and Te atoms, the spin-orbit coupling effects should be considered. Also, as
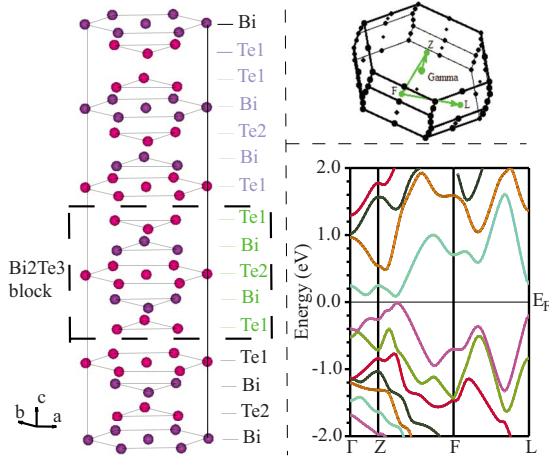
FIG. 1. (Color online) Left: $Bi_2Te_3$ hexagonal conventional cell structure; upper right: $Bi_2Te_3$ first Brillouin zone; lower right: $Bi_2Te_3$ electronic band structure along some high-symmetry lines.



FIG. 2. (Color online) Normalized phonon density of states of $Bi_2Te_3$ with respect to frequency. Heavy solid curve: computed classical interatomic potentials; light dashed curve: computed *ab initio*; dashed curve: experimental values from Ref. 20.

suggested by Larson,[13] the $p_{1/2}$ corrections which may significantly affect the electronic band structure have also been considered for the Bi $6p$ and Te $5p$ states. The calculated electronic band structure along high-symmetry lines is plotted in Fig. 1, where the band-structure profiles are similar with previous reports,[13–17] indicating that our calculation can properly describe the ground state. On the other hand, the conduction-band minima and valence-band maxima for $Bi_2Te_3$ are off the high-symmetry lines, as pointed out in Refs. 14, 16, and 17. Although it is always favorable to accurately predict the band-gap value, we did not make an effort here since our molecular dynamics simulations will be performed at the ground state.

We adopt the ABINIT code[18] to study the phonon properties of bulk $Bi_2Te_3$ and then to validate the obtained interatomic potentials by reproducing the phonon behaviors of $Bi_2Te_3$. By starting from the experimental structure,[9] the Hartwigsen-Goedecker-Hutter pseudopotential is used with local-density approximation (LDA) approximation to fully relax the unit-cell structure, while the $4 \times 4 \times 4$ shifted $k$ grid in the first Brillouin zone is adopted based on energy convergence tests. The fully relaxed structure has rhombohedral unit-cell parameters $a_R = 10.27$ Å, $\theta_R = 24.49°$ and atomic parameters $u = 0.400$, $v = 0.791$. From the fully relaxed structure, calculations based on variational density-functional perturbation theory[19] are performed and the obtained phonon density of states (phonon DOS) is plotted in Fig. 2. As seen, the *ab initio* calculations successfully reproduced the relative strength and positions of the peaks, as well as the cutoff frequencies in phonon DOS in comparison to experiments. Calculations at Gamma point also reveal that the eigenfrequency of $A_{1g}$ phonon mode is 1.94 THz, which is in good agreement with experimental values 1.88 THz.[21] Since *ab initio* calculation can reproduce the phonon properties of $Bi_2Te_3$, it is used to generate total ground-state energy data to allow parameterizing classical interatomic potentials for phonon transport studies, as will be shown in detail in the next section.
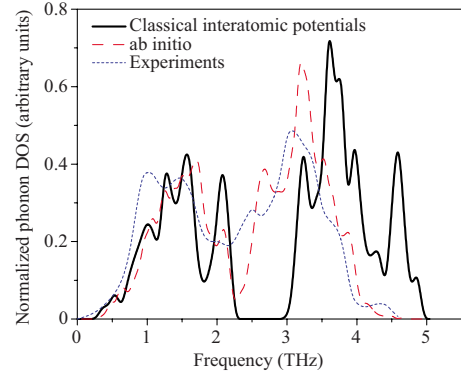
## III. CLASSICAL INTERATOMIC POTENTIALS

Appropriate classical interatomic potentials are crucial in MD predictions. The simplicity of the potentials is also important to ensure their better transferability. So far, few interatomic potentials exist in literature for $Bi_2Te_3$. Simple harmonic potentials were obtained by fitting to experiments[22,23] but they are not suitable for the calculation of lattice thermal conductivity due to the omitted anharmonic effects. The three-body potentials developed by Huang *et al.*[5] can predict the thermal conductivity quite well but the potential form is quite complicated. In light of this, we develop simpler two-body interatomic potentials which include anharmonic interactions by fitting to the energy surface from the *ab initio* calculations.

The two-body potential $\varphi(r_{ij})$ between atoms $i$ and $j$ separated by a distance $r_{ij}$ can be written in a form consisting of a short-range interaction $\varphi_s(r_{ij})$ and a Coulombic term for the long-range electrostatic interaction,

$$\varphi(r_{ij}) = \varphi_s(r_{ij}) + q_i q_j / r_{ij}, \qquad (1)$$

where $q_i$ and $q_j$ are effective charges of the ions in a partially charged model, which is more appropriate for partially covalently bonded solids such as $Bi_2Te_3$. For the Coulombic term, we have adopted the charge values obtained in Kullmann's work[23] which are 0.38, −0.26, and −0.24 for Bi, Te1, Te2 atoms, respectively.

For the short-range interactions, we chose to use the Morse potential form, which is known as a good approximation for vibrational structure of molecules

$$\varphi_s(r_{ij}) = D_e[\{1 - e^{[-a(r_{ij}-r_0)]}\}^2 - 1]. \qquad (2)$$

Here, $D_e$ is the depth of the potential well, $r_0$ is the equilibrium bond distance, and $a$ is the measure of bond elasticity. Treated with care, by considering only the nearest neighbors for short-range interactions, we reached at a potential form with different cutoff distances for different pairs, while the long-range electrostatic interactions are treated by Ewald summation method[24] with uniform cutoff radius. The parameters in the potential functions are obtained by fitting to the *ab initio* calculated total-energy surface. The fitting is a mul-

TABLE I. The short-range interatomic pair potential for $Bi_2Te_3$. Here $r$ is the separation between atom pair and $r_c$ is the cutoff distance.

| Interaction | $D_e$ (eV) | $a$ (1/Å) | $r_0$ (Å) | $r_c$ (Å) |
|---|---|---|---|---|
| Te1-Bi | 0.975 | 1.285 | 3.089 | 4.0 |
| Te2-Bi | 0.582 | 1.257 | 3.251 | 4.0 |
| Te1-Te1 | 0.076 | 1.675 | 3.642 | 5.0 |
| Bi-Bi | 0.085 | 2.212 | 4.203 | 5.5 |
| Te2-Te2 | 0.066 | 2.876 | 4.312 | 5.0 |
| Te1-Te2 | 0.807 | 0.731 | 4.497 | 5.5 |

tivariable fitting procedure done with GULP.[25]

Using the parameterized potentials, we optimize the crystal structure and predict the elastic properties, and then compare the results to experimental data. Such procedures iterate until the predicted results agree with experimental data well. The final optimized parameters are listed in Table I. First of all, it can be seen that Te1-Te1 bond has relatively small bond energy but intermediate force constant, which originates from the combined nature of van der Waals interactions across adjacent Te1-Te1 layers and covalent bonds within the same layer. The combination of Te1-Te1 bond with electrostatic repulsive interactions between Te1 atoms results in an ioniclike interaction as also observed by Huang and Kaviany.[5] On the other hand, the bond energies of the cross plane Te1-Bi, Te2-Bi, and Te1-Te2 bonds are higher than other bonds, which indicates that these bonds are more ionic. However, the force constants of these bonds are generally smaller, which is consistent with the fact that the elastic constant $C_{33}$ is less than $C_{11}$. As a result, the vibrations in the cross-plane direction is expected to be weaker than the in-plane direction and so is the heat transport through phonon channels.

By employing the fitted classical potentials, the elastic constants and bulk modulus are obtained and compared to Huang's results and experimental data as listed in Table II. It is seen that the computed elastic properties are in overall good agreement with experiments, indicating that the poten-

TABLE II. Comparison of computed elastic constants $C_{\alpha\beta}$ and bulk modulus $B$ with other works and experiments at temperature 0 K.

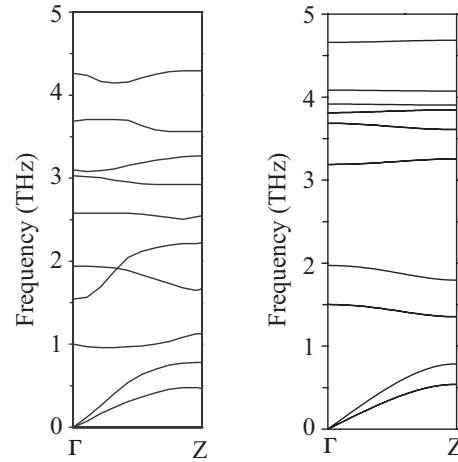| | Ultrasonic experiment[a] | Many-body potential MD[b] | This work |
|---|---|---|---|
| $C_{11}$ | 74.4 | 69.0 | 75.4 |
| $C_{12}$ | 29.2 | 21.6 | 23.7 |
| $C_{14}$ | 15.4 | 12.3 | 11.0 |
| $C_{33}$ | 51.6 | 54.8 | 49.3 |
| $C_{44}$ | 29.2 | 28.8 | 23.5 |
| $C_{66}$ | 26.2 | 26.7 | 25.8 |
| $B$ | 39.5 | 34.4 | 37.3 |

[a]Reference 22.
[b]Reference 5.



FIG. 3. Phonon dispersion of $Bi_2Te_3$ computed using classical interatomic potentials along high-symmetry direction $\Gamma-Z$ (right) compared to experimental phonon dispersion from Ref. 20 (left).

tials can well describe the harmonic behaviors of $Bi_2Te_3$. Also, by computing the dynamical matrix in GULP package, the phonon DOS is predicted and shown in Fig. 2 in comparison with both the previously obtained phonon DOS from *ab initio* calculations and the experiments.[20] It is seen that the classical interatomic potentials successfully reproduced the lower-frequency acoustic portion of the phonon DOS as compared to both *ab initio* calculations and experiments in both relative strength and positions. However, on the other hand, the predicted position for the second major peak is relatively higher than the experimental value while the relative strength of those peaks around the second major peak is in good agreement with *ab initio* calculations. Also, the phonon cutoff frequency is higher than that from both *ab initio* results and experiments. A closer look at the phonon dispersions, as shown in Fig. 3, shows the comparison between phonon dispersion computed from classical interatomic potentials and the experimental relations. it is seen that the acoustic-phonon modes of $Bi_2Te_3$ are well reproduced while optical-phonon modes are generally overestimated. Especially for higher-frequency modes, the overestimation is significant and results in a gap between 2.3 and 3 THz, which is not seen in either experiment or *ab initio* calculations. This is probably due to the oversimplified rigid-ion model that ignores the polarization in Bi and Te atoms. This simplification might greatly affect the dispersion relation of optical-phonon modes, which should be considered as a limitation of our classical potentials model, and core-shell model might improve the phonon-dispersion relations. Despite the relatively poor capability of the interatomic potentials in reproducing optical-phonon dispersions, the dispersion of acoustic-phonon modes are well predicted. Therefore, we expect that the interatomic potentials can predict the lattice thermal conductivity of $Bi_2Te_3$ reasonably well since the thermal transport is dominated by acoustic-phonon modes while the optical-phonon contributions are generally negligible.

## IV. MOLECULAR DYNAMICS SIMULATIONS ON LATTICE THERMAL CONDUCTIVITY

Phonon thermal conductivity of solids can be effectively predicted using equilibrium molecular dynamics simulations

together with the Green-Kubo linear-response formulation.[26] For the anisotropic system of interest here, phonon thermal conductivity is given by[27]

$$\kappa_{l,\alpha} = \frac{1}{k_B V T^2} \int_0^\infty \langle S_\alpha(t) \cdot S_\alpha(0) \rangle dt, \quad \alpha = x, y, z, \quad (3)$$

here $V$ is the volume of simulation domain, $T$ is the temperature, $\langle S_\alpha(t) \cdot S_\alpha(0) \rangle$ is the heat current autocorrelation function (HCACF) along a particular direction, and $\langle \dots \rangle$ means the ensemble average. For a pair potential, the heat current is expressed as

$$\mathbf{S} = \sum_i e_i \mathbf{v}_i + \frac{1}{2} \sum_{i,j} (\mathbf{F}_{ij} \cdot \mathbf{v}_i) \mathbf{r}_{ij}, \quad (4)$$

where $\mathbf{v}_i$ is the velocity of particle $i$, $\mathbf{F}_{ij}$ is the forces between two particles, and $\mathbf{r}_{ij}$ is the separation. The MD simulations were performed with a system consisting of $6 \times 6 \times 1$ hexagonal unit cells and involving 540 atoms. The simulations in larger simulation domain produced very similar results. The temperatures considered were from 150 to 500 K with an interval of 50 K. The time step was chosen as 0.25 fs. The Verlet leapfrog algorithm was adopted for the calculation while the Nose-Hoover thermostat was used to control the system temperature. The system was first simulated in an constant number of atoms, volume, and temperature ensemble for 250 ps to ensure it reached equilibrium at the desired temperature; then, it was switched into an NVE ensemble and ran for 250 ps to arrive in equilibrium, after which HCACFs were computed and outputted. At each temperature point, nine runs of MD simulations were done to average and minimize statistical fluctuations, while in each run, 2000 ps raw heat current data were obtained for the calculation of HCACFs. Since the Debye temperature of $Bi_2Te_3$ is only 155K,[28] we do not make any attempt to include quantum effects for the temperature range of our interest.

Based on the observed shape of the HCACF, and by realizing the optical-phonon contribution will mostly only account for the large oscillations in HCACFs and is temperature independent which is not the focus of current interest, the HCACFs can be fitted to a sum of two exponential functions as[5,29]

$$\langle S_\alpha(t) \cdot S_\alpha(0) \rangle = A_{ac,sh,\alpha} \exp(-t/\tau_{ac,sh,\alpha})$$
$$+ A_{ac,lg,\alpha} \exp(-t/\tau_{ac,lg,\alpha}), \quad (5)$$

then the lattice thermal conductivity could be obtained by performing direct integrals of these exponential functions. Here the subscripts $ac, sh$ and $ac, lg$ denote acoustic short-range phonon and acoustic long-range phonon, respectively. For $Bi_2Te_3$, the contribution from acoustic phonons has been immersed in the optical-phonon oscillations while it has been shown that the contribution of optical phonons to the thermal conductivity of $Bi_2Te_3$ is negligible,[5] however, the huge oscillations in HCACF do make the fitting to HCACF with exponential decay form very difficult. Fortunately, on the other hand, the lattice thermal conductivity can be defined as the $\omega \rightarrow 0$ limit of the Fourier transform of the HCACF,
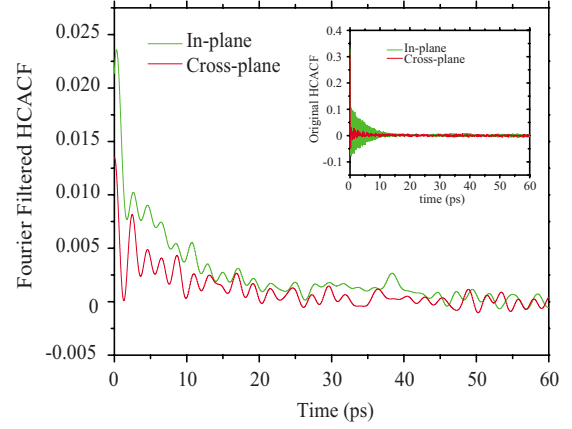


FIG. 4. (Color online) Typical HCACF with respect to time at 300 K before (insert) and after Fourier filtering.

$$\kappa_{l,\alpha} = \lim_{\omega \rightarrow 0} \frac{1}{k_B V T^2} \int_0^\infty \langle S_\alpha(t) \cdot S_\alpha(0) \rangle e^{i\omega t} dt. \quad (6)$$

Therefore, in order to better extract the acoustic-phonon signals, a Fourier low-pass filter with the cutoff frequency 0.5 THz can be used to remove the high-frequency optical-phonon components in the HCACF and fit the low-frequency acoustic part using the two-stage exponential decay function. Although, as pointed out by Volz and Chen,[30] small cutoff frequency will affect the accuracy of the outcomes due to the fact that the finite size of the simulation domain does not allow very long-wavelength phonons to physically present, an appropriate choice of the cutoff frequency which allows exponential decay fitting to HCACF is expected to give accurate lattice thermal conductivity value. In the present studies, the scale of the simulation domain is $6a$, where $a$ is the lattice constant. By assuming that the longest phonon wavelength that can exist in the domain is about the same scale of the domain, then only phonon modes within $(1/6) \times 2\pi/a$ about the Brillouin-zone center are inaccurate, which correspond to phonon frequencies less than 0.2 THz. Thus, with the choice of cutoff frequency 0.5 THz, the correctness of the results obtained here is not expected to be affected. Indeed, by testing different choices of cutoff frequencies from 0.5 to 1.5 THz, only less than 1% difference in the results is seen, which falls into the standard error from the fitting.

Figure 4 shows the typical HCACF obtained as function of time before (inset of Fig. 4) and after applying Fourier filter. As it is seen, after fast Fourier transform, the large oscillations are greatly removed and exponential decay behavior of the HCACF has emerged, which allows for the two-stage exponential decay fitting mentioned earlier. From the fitting, the typical relaxation time for short-range acoustic phonons in cross-plane direction is 0.4 ps while in in-plane direction is 0.8 ps, and they are temperature independent. Since the short-range acoustic-phonon contributions correspond to energy transfers between neighboring atoms, the difference in the relaxation times is consistent with the fact that bond length in in-plane direction is generally larger than in cross-plane direction. The long-range acoustic-phonon contributions dominate the lattice thermal conductivity and
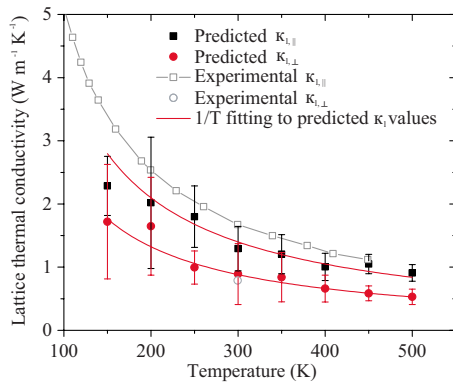
FIG. 5. (Color online) Computed temperature-dependent in-plane and cross-plane lattice thermal conductivity compared with the experimental data (Ref. 31).

roughly exhibit $T^{-1}$ dependence in both directions, indicating that the dominant phonon-scattering mechanism should be three-phonon Umklapp process in the temperature range of interest in both directions, which limits the thermal conductivity of the bulk $Bi_2Te_3$. The relaxation times for long-range acoustic phonons in cross-plane direction are generally smaller than in in-plane direction over the temperature range, indicating Umklapp scattering is larger in the cross-plane direction. In Fig. 5, the plot of $\kappa_l$ vs. temperature is shown and compared to experiments, good overall agreement is seen in both directions. Compared to Huang and Kaviany's results,[5] the lattice thermal conductivity predicted from their classical potentials are generally larger than the values obtained here for both directions, which could be attributed to the fact that the three-body interactions in their potentials might bring in more rigid bonds. On the other hand, the predicted in-plane lattice thermal conductivities are about 15–20% less than the experimental values. This underestimation indicates the bond strength in in-plane direction produced by the fitted classical potentials might be less than in reality. Despite the underestimation, the fitted potential successfully reproduced the relative strengths of the lattice scattering in in-plane and cross-plane directions together with their temperature dependence. As a result, the lattice thermal conductivities in the cross plane is smaller than in the in-plane values, indicating that the lattice scattering in the cross plane is larger. This is due to the different anharmonicities originated from different bonding natures along the two directions (as can be seen in the fitted potentials) and difference in mass of Bi and Te atoms which can result in large mismatch of available phonon modes of different atoms in the cross plane, which induces stronger lattice scattering.

## V. DISCUSSIONS AND CONCLUSIONS

In conclusion, we use the pseudopotential method based on density-functional theory with LDA to characterize the electronic structures of $Bi_2Te_3$. We then develop the two-body interatomic potentials based on which the calculated elastic constants and phonon DOS agree well with the experiments and *ab initio* calculations, indicating that the developed potentials are suitable in describing the harmonic behaviors of $Bi_2Te_3$ and can well capture the phonon transport nature within. By utilizing this fitted potential, molecular dynamics simulations are performed and the lattice thermal conductivities are reproduced over a temperature range from 150 to 500 K using Green-Kubo method, which generally reveal an Umklapp process for the bulk. Close agreement with experiment is seen. The obtained results suggest that the low lattice thermal conductivity of $Bi_2Te_3$ is a result of weak bondings among Bi and Te atoms while the anisotropic phonon transport in $Bi_2Te_3$ stems from the difference in elastic and anharmonic properties along in-plane and cross-plane directions. Besides the success of our simple two-body interatomic potential form in reproducing thermal transport process in bulk, it can also allow for further phonon transport studies in $Bi_2Te_3$-based nanostructures and alloys, which will be reported in subsequent works.

*ruan@purdue.edu

[1] R. Venkatasubramanian, E. Siivola, and B. O'Quinn, Nature (London) **413**, 597 (2001).

[2] J. Zhou, C. Jin, J. Seol, X. Li, and L. Shi, Appl. Phys. Lett. **87**, 133109 (2005).

[3] B. Poudel, Q. Hao, Y. Ma, Y. Lan, A. Minnich, B. Yu, X. Yan, D. Wang, A. Muto, D. Vashaee, Xiaoyuan Chen, Junming Liu, Mildred S. Dresselhaus, Gang Chen, and Zhifeng Ren, Science **320**, 634 (2008).

[4] Y. Q. Cao, X. B. Zhao, T. J. Zhu, X. B. Zhang, and J. P. Tu, Appl. Phys. Lett. **92**, 143106 (2008).

[5] B.-L. Huang and M. Kaviany, Phys. Rev. B **77**, 125209 (2008).

[6] A. Pattamatta and C. K. Madnia, Int. J. Heat Mass Transfer **52**, 860 (2009).

[7] R. Yang and G. Chen, Phys. Rev. B **69**, 195316 (2004).

[8] D. Lacroix, K. Joulain, D. Terris, and D. Lemonnier, Appl. Phys. Lett. **89**, 103104 (2006).

[9] P. W. Lange, Naturwiss. **27**, 133 (1939).

[10] D. Singh, *Planewaves, Pseudopotentials, and the LAPW Method* (Kluwer Academic, Boston, 1994).

[11] W. Kohn and L. Sham, Phys. Rev. **140**, A1133 (1965).

[12] P. Blaha, K. Schwarz, G. Madsen, D. Kvasnicka, and J. Luitz, *WIEN2K, An Augmented Plane Wave Plus Local Orbitals Program for Calculating Crystal Properties* (Vienna University of Technology, Austria, 2001).

[13] P. Larson, Phys. Rev. B **68**, 155121 (2003).

[14] S. J. Youn and A. J. Freeman, Phys. Rev. B **63**, 085112 (2001).

[15] T. J. Scheidemantel, C. Ambrosch-Draxl, T. Thonhauser, J. V.

Badding, and J. O. Sofo, Phys. Rev. B **68**, 125210 (2003).

[16] M. Kim, A. J. Freeman, and C. B. Geller, Phys. Rev. B **72**, 035205 (2005).

[17] P. Larson, Phys. Rev. B **74**, 205113 (2006).

[18] http://www.abinit.org/

[19] C. Lee and X. Gonze, Phys. Rev. B **51**, 8610 (1995).

[20] H. Rauh, R. Geick, H. Kohler, N. Nucker, and N. Lehner, Solid State Phys. **14**, 2705 (1981).

[21] A. Q. Wu and X. Xu, Appl. Phys. Lett. **92**, 011108 (2008).

[22] J. O. Jenkins, J. A. Rayne, and R. W. Ure, Phys. Rev. B **5**, 3171 (1972).

[23] W. Kullmann, G. Eichhorn, H. Rauh, R. Geick, G. Eckold, and U. Steigenberger, Phys. Status Solidi B **162**, 125 (1990).

[24] P. P. Ewald, Ann. Phys. (Leipzig) **64**, 253 (1921).

[25] J. D. Gale, J. Chem. Soc., Faraday Trans. **93**, 629 (1997).

[26] R. Kubo, M. Toda, and N. Hashitsume, *Statistical Physics II: Nonequilibrium Statistical Mechanics* (Springer-Verlag, Berlin, 1991).

[27] D. A. McQuarrie, *Statistical Mechanics* (University Science Books, Sausalito, 2000).

[28] G. E. Shoemake, J. A. Rayne, and R. W. Ure, Jr., Phys. Rev. **185**, 1046 (1969).

[29] A. J. H. McGaughey and M. Kaviany, Int. J. Heat Mass Transfer **47**, 1799 (2004).

[30] S. G. Volz and G. Chen, Phys. Rev. B **61**, 2651 (2000).

[31] C. B. Satterthwaite and J. R. W. Ure, Phys. Rev. **108**, 1164 (1957).